UPPSALA
UNIVERSITET

IT 13 066
Examensarbete 15 hp
September 2013

Fatigue Analysis of Threaded Holes

A project performed at ÅF using static structural analysis in ANSYS

Andreas Olsson
Joel Sundström

Institutionen för informationsteknologi
Department of Information Technology

UPPSALA
UNIVERSITET

Teknisk- naturvetenskaplig fakultet
UTH-enheten

Besöksadress:
Ångströmlaboratoriet
Lägerhyddsvägen 1
Hus 4, Plan 0

Postadress:
Box 536
751 21 Uppsala

Telefon:
018 – 471 30 03

Telefax:
018 – 471 30 00

Hemsida:
http://www.teknat.uu.se/student

Abstract

Fatigue Analysis of Threaded Holes

Andreas Olsson and Joel Sundström

The effect of a plain hole on the fatigue properties of a body undergoing uniaxial loading is a well-studied area. However, for the case of threaded holes that are not being used together with a bolt, little can be found in the literature. In this project, stress concentration factors, Ktn, for threaded holes, following the ISO metric standard, have been calculated using finite element models in ANSYS. Based on these results, estimations of the fatigue notch factor, Ktf , for the threaded holes were derived. The magnitude of Ktf depends on how the notch sensitivity index, q, is being determined. In this project, both Neuber's and Peterson's formulas were used as estimates of q and a comparison between the two methods was made. The stress concentration factors for the threaded holes were significantly higher than the corresponding stress concentration factors for plain holes. As the size of the hole and the surrounding body was increased, Ktn decreased. In the fatigue analysis, Peterson's formula predicted higher values of the fatigue notch factor compared to Neuber's and could therefore be useful in design purposes. Furthermore, the reduction in fatigue strength for the threaded holes, compared to the plain holes, was calculated. These results showed that the percentage decrease in fatigue strength for threaded holes was approximately the same, regardless if Neuber's or Peterson's estimation of q was used. The reduction in fatigue strength for threaded holes with a coarse pitch, compared to plain holes, varied from about 16 % for the smallest diameter tested (M6) to about 10 % for the biggest (M68). The corresponding reduction for threaded holes with a fine pitch varied from about 14 % for the smallest diameter (M6) to about 9 % for the biggest (M64). As the size of the hole and the surrounding body was increased, the threads' effect on the fatigue strength decreased.

Handledare: Fredrik Södergren
Ämnesgranskare: Axel Målqvist
Examinator: Jarmo Rantakokko
IT 13 066
Tryckt av: Reprocentralen ITC

Contents

1 Introduction

1.1 Background

The usage of screw threads in construction parts and building blocks is very common in the industry. Threaded holes with bolts are one of the most basic and widely used methods to connect two structural parts together. For obvious reasons, most screw threads present in various structures are being used together with a bolt. However, it is not uncommon that structural members and machine parts contain threaded holes that are not being used. Unused threaded holes often appear in situations where a machine, shaft, or engine block is modified during its life time. For example, due to technical development, some necessary modifications of industrial parts might lead to unused threaded holes. The main question sought to be answered in this project is therefore how threaded holes differ from plain holes in their effect on the fatigue properties of structural members. This question arose from a discussion between the technical consulting firm ÅF and one of their customers.

The stress distribution around circular holes is a thoroughly studied area, but for the case when the holes contain screw threads, little can be found in the literature. Irregularities such as holes, notches, shoulders, and so on, are referred to as stress raisers because they alter the way the stress is distributed in the material during loading, leading to high localized stresses. The phenomenon when such an irregularity produces high localized stresses is called stress concentration, [15]. In order to avoid devastating failures of assemblies, these stress concentrations must be accounted for in calculations and designs. A measure of the stress concentration is provided through the stress concentration factor, K_t, defined as the ratio of the peak stress in the body, σ_{max}, to some predefined reference stress, σ_{nom},

$$K_t = \frac{\sigma_{max}}{\sigma_{nom}} \tag{1}$$

The stress concentration factor is a theoretical factor meaning that it is derived from laboratory tests or based on the theory of elasticity. Today, advanced computer simulations, most often involving the finite element method, can be used to determine the stress concentration factors for practically all kinds of shapes, materials, and loads.

For the case of a uniform tension load applied to an infinite thin plate with a circular hole, seen in Figure 1, an analytical solution is possible to derive. At point A, the maximum stress is obtained and it can be expressed as

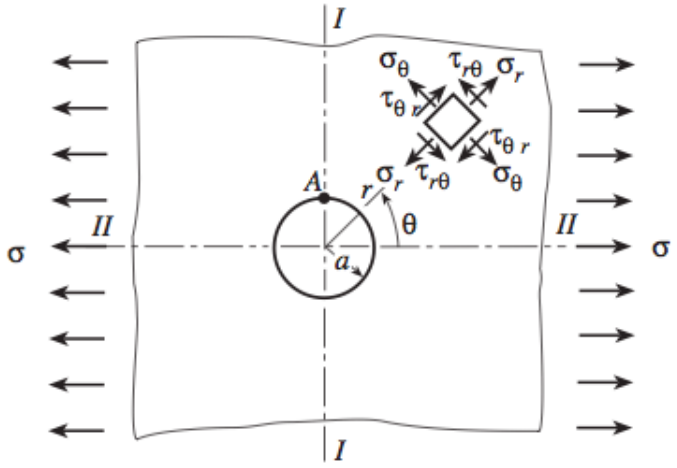

Figure 1: An infinite thin plate with a circular hole under a uniform tension load.The figure was taken from [12].

$$\sigma_{max} = 3\sigma \tag{2}$$

Here, the stress concentration factor is 3, meaning that for an applied stress σ, the resulting maximum stress at the edge of the hole will be 3σ, [12]. For simple plane stress cases like this, numerous handbooks have been written containing formulas for a wide range of shapes and loads. However, in order to conduct a three-dimensional analysis of a threaded hole in an arbitrary body, one cannot simply rely on handbooks anymore. These types of analyzes are preferably carried out in a sophisticated finite element software, for example, ANSYS.

Studies have shown that when the element containing the hole has an arbitrary thickness, the maximum stress varies on the surface of the hole across the thickness of the body, [12]. In other words, the maximum stress does not necessarily occur on the surface of the element. In fact, research has shown that the stress is slightly higher in the interior of the body (but still on the surface of the hole), [13]. According to [4], the stress concentration factor for an arbitrary thickness plate holding a through-the-thickness circular hole subjected to uniaxial tension could increase with approximately 6% compared to the reference value of 3. This depends on the ratio of the thickness of the plate to the hole radius as well as the Poisson's ratio, which is a material constant. It was also found that the stress concentration factor increased with the increase of the Poisson's ratio. The same conclusions were made in [8], where it was found that holes in three-dimensional bodies had stress concentration factors 5 % higher than the corresponding two-dimensional values. The purpose of this work is to perform analyzes, similar to the

ones described above, but for the case when the holes contain screw threads.

1.2 Goal

In this project, the stress concentration factors of threaded holes, located in a rectangular shaped body subjected to uniaxial tension, will be calculated. The results will then be used to make conclusions about the screw threads' effect on the fatigue properties of the body. All results for the threaded holes will be compared with corresponding results for plain holes and potential differences will be discussed. Focus will be on the ISO metric screw threads standard and a table, showing all relevant results for the investigated threads, will be set up. Another purpose of the project is to deliver a database to ÅF containing simulations and CAD-models of the ISO metric threaded holes.

1.3 Limitations

The results presented in this project are only valid for the design, material, load case, and boundary conditions used in these particular simulations. Even if the conclusions made here could be used as rough guidelines to similar problems, the figures should not be generally applied to problems that differ from the ones described in this report.

1.4 Methodology

The outline of the project, given by ÅF, implied that no similar computations had been done in this area, that is, fatigue analyzes of unused threaded holes. The project started with a literature study along with learning ANSYS, the software that was used for the simulations. Since the built-in threads in most CAD-programs are only cosmetic, the screw threads had to designed from scratch. This was done using the CAD-software Spaceclaim. In consultation with the supervisor at ÅF, the decision was made to design the threads in a rectangular block with the hole penetrating half the thickness. Since numerous simulations of threaded holes had to be done a script was created to speed up the process.

2 ANSYS Model

ANSYS is an engineering simulation software that is used within a wide variety of areas, for example, within the automotive, aerospace and energy industry. The software is, for example, used by putting a structure through different simulations, approximating the real scenarios of the structure, to analyze its behavior before constructing the real product.

2.1 Geometry

The geometry was constructed using the CAD-software Spaceclaim and the design of the threaded holes was based on the ISO-standards for metric screw threads, see Appendix B. Every thread is defined by its pitch (P), outer diameter (D), inner diameter (D_1), and the effective pitch diameter (D_2). The parameters and a schematic view of the standard used when designing the threaded holes can be seen in Figure 2.

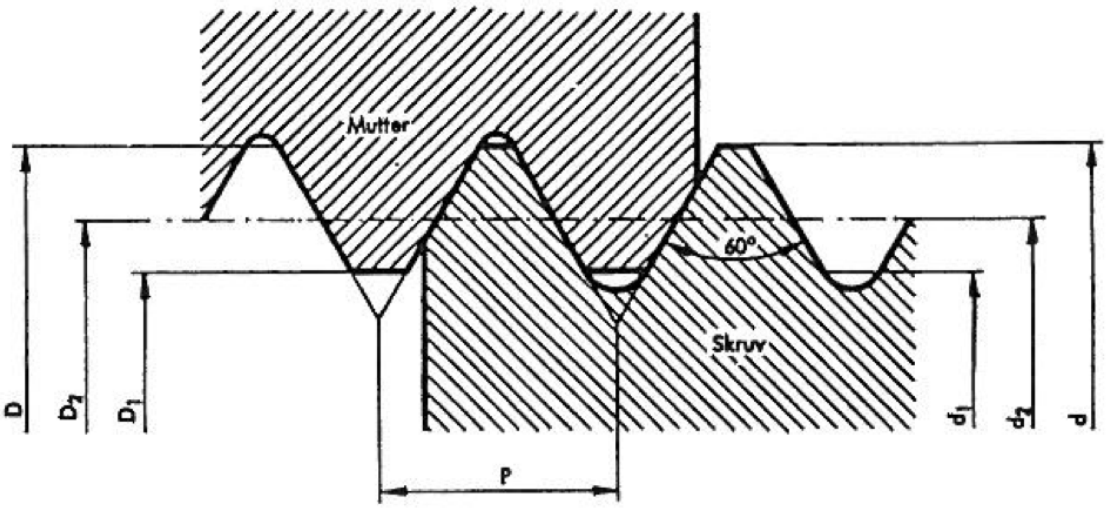

Figure 2: The standard of a M-threaded hole, ISO-standard, [6].

The values of the different parameters follow the ISO-standard and both the fine and coarse version of the threaded holes in [6] were constructed. The geometry of the solid as well as the holes were designed using the following relations, based on the threaded holes' outer diameter, D,

The surrounding body

Length of sides = 6·D
Thickness = 3·D

The threaded hole

Depth = 1.5·D

The depth was defined as the distance from the top of the hole to where the thread ended. The bottom of the hole was rounded off with a 30° angle. The relation between the threaded hole and the size of the surrounding body was based on Saint-Venant's principle. It states that an irregularity, such as a hole, with a characteristic size R will affect a region of size 3·R surrounding the irregularity, [3]. It should be noted that this principle is just a rule of thumb. A similar conclusion can be found in [12], where the effect of a hole on the surrounding stress distribution is negligible a distance $5 \cdot radius$ from the center of the hole. The size of the surrounding body was based on these two statements, however, it was made slightly bigger to be on the safe side. For each simulation, the stress at the surface of the body was recorded to make sure that the size of the body was sufficient to give a uniform distribution at the surfaces.

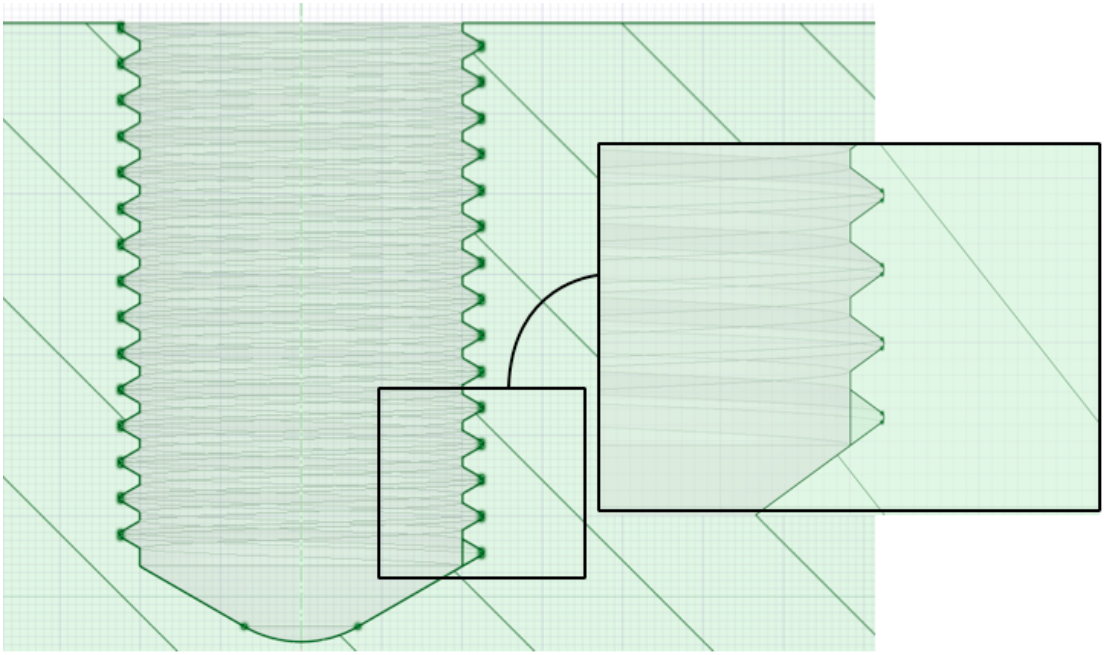

Figure 3: CAD-model of a coarse M45 including the defect down the right hand corner of the hole resulting from the sketch. The bottom of the hole was made arbitrary but followed an angle of 30° relative to the horizontal plane.

The threads were constructed by sketching the 60° profile in Figure 2 from the outer to the inner diameter. This profile was then rotated around the axis of the hole, in the shape of a helix, with the corresponding pitch. The diameter of the plain holes was the same as the inner diameter of the threaded hole. Following the standards, the profile of the thread was rounded off at the outer diameter while kept flat at the inner diameter. The whole process can be seen as cutting out the threads from the bottom of the hole to the top in Figure 3. This way of creating the geometry lead to a defect at the beginning of the thread at the bottom of the hole, since the translation could not be constructed smoothly. This defect had to be accounted for in the simulations since the sharp edges led to very high stresses, which would not appear in reality. In other words, the bottom of the hole had to be ignored when analyzing the simulations since the defect would give misleading results.

2.2 Loading and Boundary Conditions

The boundary condition applied on the body was frictionless support. With frictionless support on a surface, the nodes are restricted to in plane movement, the nodes can not move along the surface normal. In other words, where a frictionless support is applied the degrees of freedom is reduced to two. The frictionless support were applied on all sides except the unconstrained top surface and the side where the tension load was applied, which can be seen in Figure (6). A uniaxial tension load of 1 MPa was applied at one surface in the normal direction, out of the body. For each thread, two simulations were done, one with the pressure load in the x-direction and one in the y-direction. This was done to ensure that the lack of perfect symmetry would not bias the result. The tension load was defined as a pressure load in the direction normal to the surface. This was convenient since it has the same units as the stress, which made it easy to determine the stress concentration factor from equation (1).

These conditions were used to give a realistic approximation of the real problem where the threaded hole was a part of a larger body, for example, an engine block.

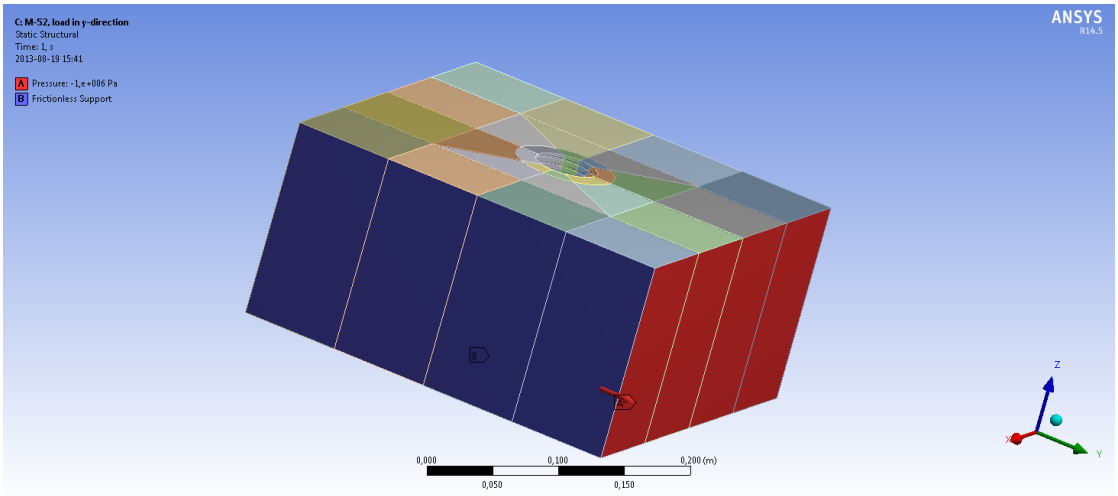

Figure 4: An applied tension load pressure in the y-direction, out of the body. The top of the body was unconstrained and the remaining sides had frictionless support.

3 Mathematical model

In this section, a brief review of the equations governing the problem will be outlined. In the mathematical model, the following assumptions are made:

- The body is elastic, that is, the solid returns to its original shape when the load is removed.
- The material is isotropic, which means that there is no characteristic orientation in the material. In other words, the stress-strain curves are independent of the orientation of the solid.
- The deformations due to the applied load are small.
- The temperature distribution in the solid is uniform, that is, $\Delta T = 0$.
- The material follows Hooke's law, which states that strain is proportional to stress.[15]

The problem to be modeled is a three-dimensional rectangular shaped body, with volume V and surface S, subjected to an external tension force P. The three unknown fields in the body are displacements u, strains ε, and stresses σ. These fields are connected through three sets of governing equations, [5]. The first set of governing equations is derived from the relation between the displacement and strain in linear elasticity. This relationship can be described by the *infinitesimal strain tensor*, ε_{ij}, which is given by

$$\varepsilon_{ij} = \frac{1}{2}(\frac{\partial u_i}{\partial x_j} + \frac{\partial u_j}{\partial x_i}) \tag{3}$$

Details about the infinitesimal strain tensor can be found in [3], but it should be noted that this measure of deformation is approximate and only suitable for small deformations of the body, which is assumed to be the case here. The second set of governing equations is the equations relating stress and strain. They are often referred to as the *constitutive equations*. In general, the constitutive equations are partial differential equations, but in the case of linear elasticity, they become algebraic, linear, and homogeneous, [5]. The stress-strain relation for an isotropic, linear elastic solid is

$$\sigma_{ij} = \frac{E}{1+v}(\varepsilon_{ij} + \frac{v}{1-2v}\varepsilon_{kk}\delta_{ij}) - \frac{E\alpha\Delta T}{1-2v}\delta_{ij} \tag{4}$$

where σ_{ij} is the Cauchy stress tensor, E is Young's modulus and v is the Poisson's ratio. Details about the Cauchy stress tensor can be found in [3]. Equation (4) is usually rewritten using the *elastic modulus tensor* C_{ijkl}, defined as

$$C_{ijkl} = \frac{E}{2(1+v)}(\delta_{il}\delta_{jk} + \delta_{ik}\delta_{jl}) + \frac{Ev}{(1+v)(1-2v)}\delta_{ij}\delta_{kl} \tag{5}$$

Using the elastic modulus tensor together with the assumption that $\Delta T = 0$, equation (4) breaks down to

$$\sigma_{ij} = C_{ijkl}\varepsilon_{kl} \tag{6}$$

For static problems, the internal equilibrium equations must be satisfied

$$\frac{\partial \sigma_{ij}}{\partial x_i} + \rho_0 b_j = 0, \quad \text{in V} \tag{7}$$

where ρ_0 is the mass density of the solid and b_j is the internal body force. The equilibrium equations are derived from the linear momentum balance equations and make up the third set of governing equations, [3]. On three sides of the body, the displacements are restricted to in-plane movements, that is, the boundaries cannot move in the direction of their surface normal. This means that some components of the displacements on the boundaries of the solid are known. This forms the displacement boundary conditions

$$u_i = \hat{u}_i, \quad \text{on } S_u \tag{8}$$

where S_u denotes the surfaces on the body where displacements are prescribed. On one side of the solid, a tension force is applied in the direction of the surface normal, which means that on this boundary, some components of stress are known. This forms the stress boundary conditions

$$\sigma_{ij} n_j = \hat{t}_i, \quad \text{on } S_t \tag{9}$$

where n_j is the surface normal, $\hat{t}_i$ is the prescribed tractions, and S_t denotes the surface where the load is applied. It is now possible to summarize the governing equations for the problem using equations (3), (6), (7), (8), and (9)

$$\begin{cases} \varepsilon_{ij} = \dfrac{1}{2}\left(\dfrac{\partial u_i}{\partial x_j} + \dfrac{\partial u_j}{\partial x_i}\right) & \\ \sigma_{ij} = C_{ijkl}\varepsilon_{kl} & \\ \dfrac{\partial \sigma_{ij}}{\partial x_i} + \rho_0 b_j = 0, & \text{in V} \\ u_i = \hat{u}_i, & \text{on } S_u \\ \sigma_{ij} n_j = \hat{t}_i, & \text{on } S_t \end{cases} \tag{10}$$

The problem can be stated as:

Given the shape of the solid in its unloaded condition, the elastic constants for the solid (C_{ijkl}), the mass density and the body force distribution (b) acting on the solid, calculate the displacements, strains, and stresses satisfying the governing equations in (10).

To solve three-dimensional linear elastic problems analytically is complex and will not be covered here. However, some general solution technique, like the *Papkovich-Neuber potential representation*, could be used to find analytical solutions to the problem above, [3]. As stated earlier, the computer software ANSYS was used in this project. It solves the above problem with the finite element method, which will be described briefly in the following section.

4 Finite Element Analysis

4.1 Principle of virtual work

The principle of virtual work can be used to find the strains and stresses in an elastic body assuming small changes in the displacement. The principle is based on that a little change in the internal work must be compensated by an identical change in external work due to applied loads, [1]. The equations in equation (11) are used by ANSYS to solve for strains and stresses. Using matrix calculus and discretizing to formulate the equations, equation (7), (6) and (3) can be written as

$$\begin{aligned} \mathbf{D}^T\boldsymbol{\sigma} + \bar{\mathbf{p}}_V = \mathbf{0} \quad & \text{Equilibrium equations} \\ \boldsymbol{\sigma} = \mathbf{E}\boldsymbol{\varepsilon} \quad & \text{Constitutive equations} \\ \boldsymbol{\varepsilon} = \mathbf{D}\mathbf{u} \quad & \text{Strain-displacement relationship} \end{aligned} \tag{11}$$

where $\mathbf{D}$ is the differential matrix operator,

$$\mathbf{D}^T = \begin{bmatrix} \frac{\partial}{\partial x} & 0 & 0 & \frac{\partial}{\partial y} & \frac{\partial}{\partial z} & 0 \\ 0 & \frac{\partial}{\partial y} & 0 & \frac{\partial}{\partial x} & 0 & \frac{\partial}{\partial z} \\ 0 & 0 & \frac{\partial}{\partial z} & 0 & \frac{\partial}{\partial x} & \frac{\partial}{\partial y} \end{bmatrix} \tag{12}$$

The equations in equation (11) can be combined into a system of differential equations with the displacements in the elastic body, $\mathbf{u}$, as unknowns

$$\mathbf{D}^T\mathbf{E}\mathbf{D}\mathbf{u} + \bar{\mathbf{p}}_V = \mathbf{0} \tag{13}$$

where $\bar{\mathbf{p}}_V$ is the body force acting on the body. The boundary conditions for the governing equations stated in Equation (9), natural force boundary conditions, and equation (8), essential displacement boundary conditions, that follows from equilibrium conditions can be expressed in the following discrete way, corresponding to equation (13),

$$\begin{aligned} \mathbf{A}^T\boldsymbol{\sigma} = \bar{\mathbf{p}}_S \quad & \text{on } S_t \\ \mathbf{u} = \bar{\mathbf{u}} \quad & \text{on } S_u \end{aligned} \tag{14}$$

where $\bar{\mathbf{p}}_S$ contains the surface loads and $\bar{\mathbf{u}}$ the given displacements. The allowed displacements are limited by these boundary conditions. The matrix, $\mathbf{A}^T$, is called

the transformation matrix and contains the components of the normal unit vector on the surface of the body and is defined as

$$\mathbf{A}^T = \begin{bmatrix} n_x & 0 & 0 & n_y & n_z & 0 \\ 0 & n_y & 0 & n_x & 0 & n_z \\ 0 & 0 & n_z & 0 & n_x & n_y \end{bmatrix} \tag{15}$$

Equation (13) together with the corresponding boundary conditions in equation (14), allowing only small changes, $\delta\mathbf{u}$, in the displacements, gives the equation that represents the principle of virtual work,

$$\underbrace{\int_V \delta\boldsymbol{\varepsilon}^T \boldsymbol{\sigma} dV}_{\text{virtual work of internal forces}} - \underbrace{\int_V \delta\mathbf{u}^T \bar{\mathbf{p}}_V dV - \int_{S_p} \delta\mathbf{u}^T \bar{\mathbf{p}}_S dS}_{\text{virtual work of external forces}} = 0 \tag{16}$$

also known as the weak form of the discrete equation describing the governing equations, equation (13), [12]. The problem can be stated as: *Find the small displacements* $\mathbf{u}$ *such that the work done by the external forces equals the work done by the internal forces.*

4.2 Shape functions

The finite element method, FEM, can be used to approximate the weak form, which is done by discretization. Discretizing the structure can be referred to as meshing, which is described in Section 5. Meshing implies that shape functions are necessary in order to describe the displacements between the nodes. Shape functions can also be called interpolation functions, which only depends on the position in the element and the unknown nodal displacements. Polynomials are often used as shape functions to approximate the FE solution to the real problem. For a particular element, the displacements of the points within the element, $\mathbf{u}$, can be approximated by, where k is the nodes describing the element,

$$\mathbf{u} \approx \sum_k \mathbf{N}_k \mathbf{v}_k^e = [\mathbf{N}_1, \mathbf{N}_2, ...] \begin{Bmatrix} \mathbf{v}_1 \\ \mathbf{v}_2 \\ \vdots \end{Bmatrix}^e = \mathbf{N}\mathbf{v}^e \tag{17}$$

where $\mathbf{v}^e$ contains the nodal displacements of the nodes representing the element and $\mathbf{N}$ contains predescribed functions of position, [16]. Using the approximation

of $\mathbf{u}$ for one element, e, along with the equation of virtual work, equation (16), one gets the short form of the equilibrium equation,

$$\mathbf{k}^e\mathbf{v}^e = \bar{\mathbf{p}}^e + \mathbf{p}^e \tag{18}$$

where $\mathbf{k}^e$ is the element stiffness matrix, $\bar{\mathbf{p}}^e$ is the element load vector, and $\mathbf{p}^e$ contains the internal nodal forces. For more details see [12]. In order to solve the elasticity problem for the whole structure one has to assemble the element equations for all elements, which will result in a system of linear equations. Following the principle of virtual work, the work done by all elements must equal the total work. Hence, the element nodal displacements must be consistent with the system nodal displacements and they are related as

$$\mathbf{v}^e = \mathbf{a}^e\mathbf{v} \tag{19}$$

where $\mathbf{v}$ contain the system nodal displacements and $\mathbf{a}^e$ is the global kinematic matrix. The global kinematic matrix relates the element nodal displacements to the system nodal displacements by the component values, one or zero. The virtual work of the whole system is the sum of the virtual work of all the elements, which, along with equilibrium requirements, results in the system of linear equations that describes the structural behavior

$$\mathbf{K}\mathbf{v} = \bar{\mathbf{p}} \tag{20}$$

$\mathbf{K}$ is the system stiffness matrix and $\bar{\mathbf{p}}$ is the system load vector, which respectively can be described as

$$\mathbf{K} = \sum_e \mathbf{a}^{eT}\mathbf{k}^e\mathbf{a}^e \tag{21}$$

and

$$\bar{\mathbf{p}} = \sum_e \mathbf{a}^{eT}\bar{\mathbf{p}}^e \tag{22}$$

where e indicates summation of all elements. Details about the derivation of the matrices can be found in [12], but note that $\mathbf{p}^e$ disappears due to the equilibrium in internal forces between element e and its neighboring elements.

5 Meshing

Using finite elements to approximate a real problem implies that a mesh must be generated, meaning that the body is divided into smaller elements. The meshing of a geometry can be done in different ways, using different kind of techniques. Thus, there are some conditions that needs to be satisfied in order to receive a convergent and accurate mesh

- Compatibility - is satisfied if the neighboring elements have the same nodes, and the coordinates and displacements here are described by the same interpolation functions.
- Completeness - the elements' displacement functions must represent the rigid body displacement and the constant strain states.

Apart from these conditions one has to find a balance between accuracy and computational time, since increasing the number of nodes will increase the computational time, [1]. The necessary density of the mesh depends on the shape of the geometry. Complex geometries with, for example, sharp angles demand a mesh with higher density in order to get a good approximation of the geometry. The majority of the body was approximated by hexahedral elements due to its rectangular shape. Since the threads had a complex geometry, approximating them with hexahedral elements appeared difficult and a cylindrical volume was thereby constructed around the hole. The volume, including the screw threads, was approximated by tetrahedral elements to capture the shape of the screw threads more accurately.

Assuming beforehand that the stress most certainly had its maximum at the surface of the hole since that is the case for plain holes according to [12], a mesh with smaller elements was generated in the cylindrical volume along with a refined mesh on the surface, see Figures 5 and 6. The elements were gradually done smaller from the boundaries towards the center of the hole maintaining the smooth transition between the meshes, see Figure 6, [9]. Due to the increase in computational time the elements became gradually larger when increasing the size of the threaded hole. Despite the increase of the element size, the total number of nodes in the body increased at the same time due to the expanding volume of the body. This resulted in a decrease of the number of nodes per unit volume. A general convergence study was difficult to construct due to the increasing volume of the body. The mesh was thereby generated based on the mesh from the previous threaded hole and in those situation the generated mesh was questionable, a h-refinement was done. h-refinements was done by reducing the element size, [12].

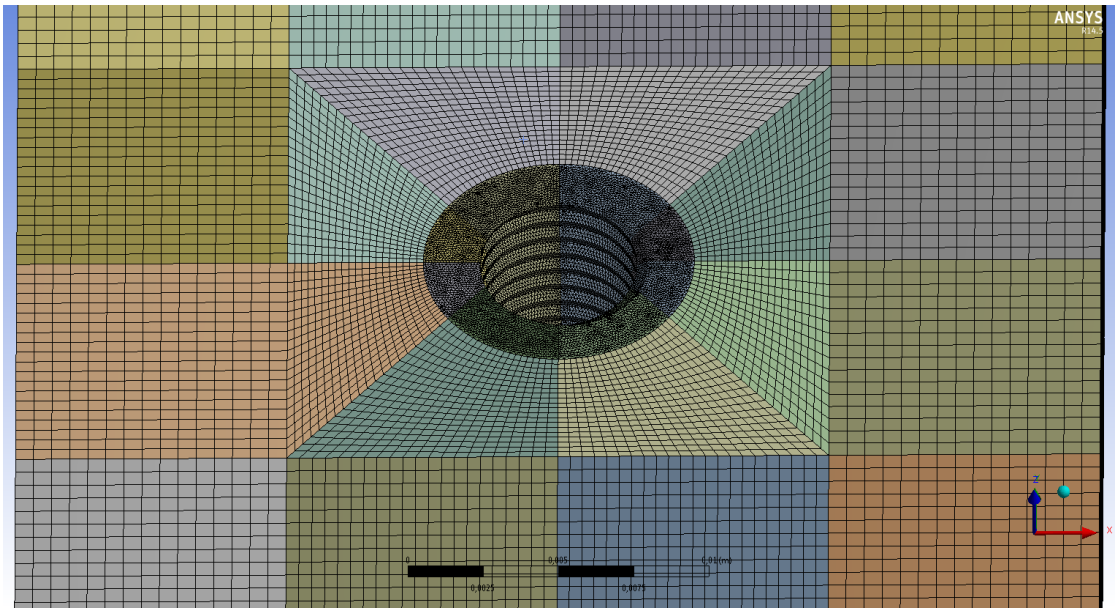

Figure 5: Mesh generated for a M6 including the partitioning of the body. All parts besides the inner cylinder, surrounding the hole, contain hexahedral elements.

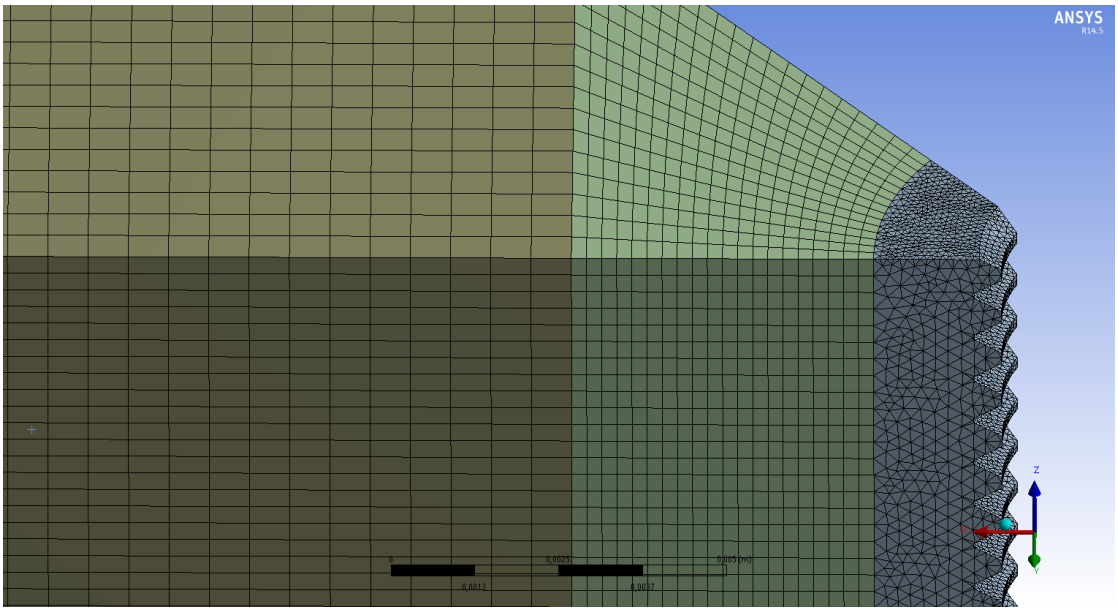

Figure 6: Mesh generated for a M6 with smooth transitions of the mesh density between the parts.

6 Stress and Fatigue Analysis

The stress distribution around a circular plain hole, located in an infinite thin plate subjected to uniaxial loading, was discussed briefly in Section 1. The stress concentration factor for such a geometry was found to equal 3 in theory. For the full three-dimensional model investigated in this project, a straight forward analytical solution was not available. Since the holes investigated did not penetrate the whole thickness of the body and the set of boundary conditions used differed from any other research made, the reference value of 3 of the stress concentration factor was not relevant. Therefore, the stress concentration factors for the threaded holes had to be compared with corresponding calculations for plain holes, using the same boundary conditions.

When calculating the stress concentration factor from equation (1), one has to define what measure to use for σ_{max} and σ_{nom}. According to [12], the maximum stress should be taken as the peak stress in the body, while the reference stress can be based on either the gross cross-sectional area or the net cross-sectional area of the body. When the reference stress is based on gross cross-sectional area, the stress concentration factor is referred to as K_{tg}, and when it is based on the net cross-sectional area, the stress concentration factor is referred to as K_{tn}. They are defined as

$$K_{tg} = \frac{\sigma_{max}}{\sigma} \tag{23}$$

where σ_{max} is the maximum stress at the edge of the hole, σ is the stress on a gross cross-section far from the hole, and

$$K_{tn} = \frac{\sigma_{max}}{\sigma_n} \tag{24}$$

where σ_n is the net stress expected when accounting for the cross-sectional area of the hole. In this particular case, the relation between the two measures can be written as

$$K_{tn} = \frac{\sigma_{max}}{\sigma}\frac{\sigma}{\sigma_n} = K_{tg}\frac{\sigma}{\sigma_n} = K_{tg}\left(1 - \frac{h'd}{hH}\right) \tag{25}$$

where d is the hole diameter, h' is the depth of the hole, h is the thickness of the element, and H is the width of the element according to Figure 7.

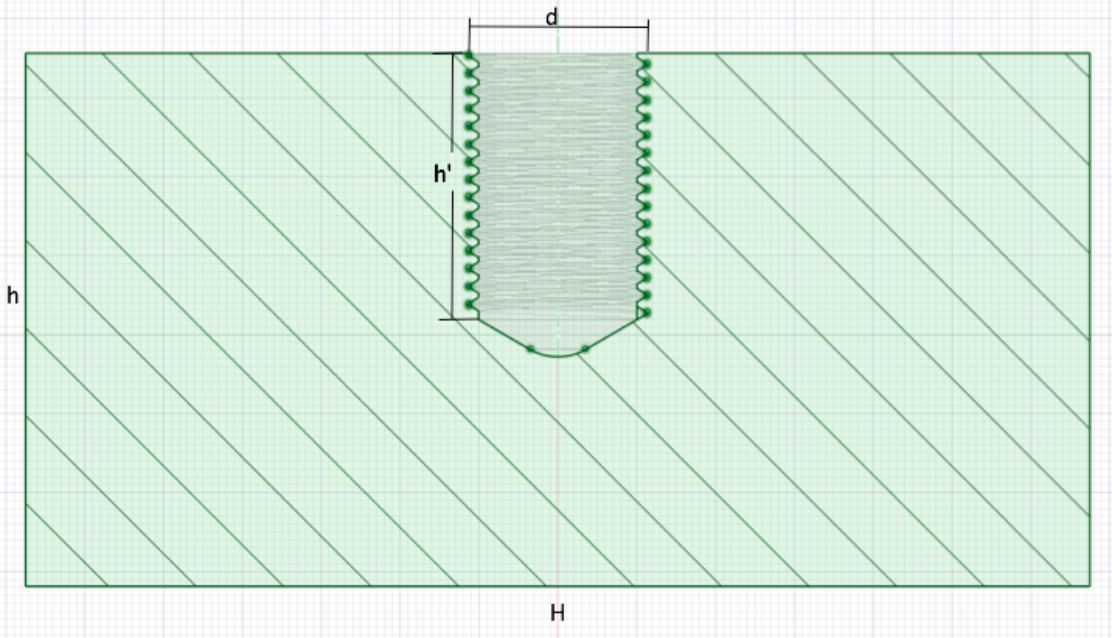

Figure 7: The cross-sectional area of the solid at the center of the hole.

Note that a simplification was made here, where the cross-sectional area of the threaded holes was assumed to be of rectangular shape. This was motivated by the fact that the threaded holes' outer diameter was used in equation (25), which means that the excluded cross-sectional area of the bottom of the hole was accounted for by the cross-sectional area of the threads. The difference in the two definitions of K_t becomes evident when the relationship between the dimensions varies. However, as mentioned in Section 2.1, the relations between d, H, h', and h were kept constant in the models. Therefore, the only difference between K_{tg} and K_{tn} was a constant factor. Since $H = 2h = 4h' = 6d$, that factor became

$$K_{tn} = K_{tg}\left(1 - \frac{3}{2 \cdot 3 \cdot 6}\right) = K_{tg}\frac{11}{12} \tag{26}$$

For the plain holes, with diameters equal to the corresponding threaded holes' outer diameter, the cross-sectional area of the bottom of the hole was included. The bottom was approximated as a triangle with base angles of 30°. Therefore, after some basic trigonometry, the resulting factor for the plain holes became

$$K_{tn} = K_{tg}\left(\frac{11}{12} - \frac{1}{2\sqrt{3} \cdot 18}\right) = K_{tg}\left(\frac{11}{12} - \frac{1}{36\sqrt{3}}\right) \tag{27}$$

When stress concentration factors are used in fatigue analyzes, it is crucial to use K_{tn} and not K_{tg}, [12]. As a measure of the maximum stress in the body, *the equivalent stress*, σ_{eq}, was used. The equivalent stress is a way of summarizing all the principal stresses into one single measure of stress. It is defined as

$$\sigma_e = \sqrt{\frac{(\sigma_1 - \sigma_2)^2 + (\sigma_2 - \sigma_3)^2 + (\sigma_1 - \sigma_3)^2}{2}} \tag{28}$$

where σ_1, σ_2, and σ_3 are the principal stresses in an arbitrary point in the body, [12]. The equivalent stress is a standard output of static structural analyzes in ANSYS. For each hole dimension the maximum equivalent stress was recorded and compared to the equivalent stress at the load surface. Since the tension load, acting on one surface of the element, corresponded to 1 MPa, the nominal stress based on gross cross-sectional area, σ, was 1 MPa. Hence, K_{tg} could easily be calculated directly from the simulation results, using equation (23), and K_{tn} could then be calculated using equation (26).

In order to make conclusions about the threaded holes' effect on fatigue properties, the *fatigue notch factor* K_f had to be introduced. The fatigue notch factor is defined as

$$K_f = \frac{\text{fatigue strength of unnotched specimen}}{\text{fatigue strength of notched specimen}} \tag{29}$$

where fatigue strength is synonymous with endurance limit, that is, the level of stress for which the specimen is assumed to never fail under reversed cyclic loading. The fatigue notch factor is related to the stress concentration factor through

$$q = \frac{K_f - 1}{K_t - 1} \tag{30}$$

where q is the *fatigue notch sensitivity index* which, in general, takes values between 0 and 1. If q is 0, then $K_f = 1$, which means that the irregularity - in this case the threaded hole - has no effect on the fatigue strength of the specimen. If q is equal to 1, then $K_f = K_t$, and the threaded hole has full effect on the fatigue properties of the specimen, [2]. From equation (30), the fatigue notch factor can be expressed in terms of the stress concentration factor and the notch sensitivity index

$$K_{tf} = 1 + q(K_t - 1). \tag{31}$$

where the subscript t in K_{tf} means that it is an estimated fatigue notch factor based on a an average q value taken from a table or diagram, [10]. Equation (31) could then be used to estimate the fatigue notch factor based on the results on the stress concentration factors derived from the simulations in ANSYS. Note that K_{tn} had to be used in equation (31). The fatigue notch sensitivity has been showed to depend not only on the properties of the material itself, but also on the shape and the size of the specimen, [14]. Many studies have been made regarding this and the most common way of presenting the results is by plotting q versus r for different materials, where r is the notch radius. Different expressions for the relation between q and r can be found in the literature. In this project, two different estimates have been used to provide a comparison between the results. The first one is based on Neuber relations

$$q = \frac{1}{1 + \sqrt{\rho'/r}} \tag{32}$$

where ρ' is a material constant related to the grain size of the material and r is the notch radius (in this case the radius of the hole), [11]. According to equation (32), as r increases, so does q. In [7] a relation between the material constant $\sqrt{\rho'}$ and the tensile strength of steels was found. The diagram in Figure 8 shows that relationship. One can see that for increasing tensile strength, $\sqrt{\rho'}$ decreases, leading to an increasing notch sensitivity in equation (32). In other words, the harder the steel, the higher the notch sensitivity. The structural steel used in the simulations had an ultimate tensile strength of 460 MPa which corresponds to $66.7 \cdot 10^3$ psi. According to Figure 8, this gives an approximate value of $\sqrt{\rho'}$ of 0.095, which was used in the estimations of q for different notch radii.

The second estimate of q that was used was formulated by Peterson in [11] and is similar to the one discussed above. Here, the notch sensitivity index is related to the notch radius through

$$q = \frac{1}{1 + \alpha/r} \tag{33}$$

where α is a material constant. Again, the material constant was found to be related to the tensile strength of the specimen and a table showing that relationship can be seen in Figure 9. Given a tensile strength of $66.7 \cdot 10^3$ psi, a simple interpolation between 50 and 75 psi gives a corresponding α-value of 0.0117. This α-value was used in the calculations of q from equation (33).

In Figure 10 the difference between Neuber's and Peterson's formulations of q is illustrated for the hole dimensions investigated in this project. The graph shows

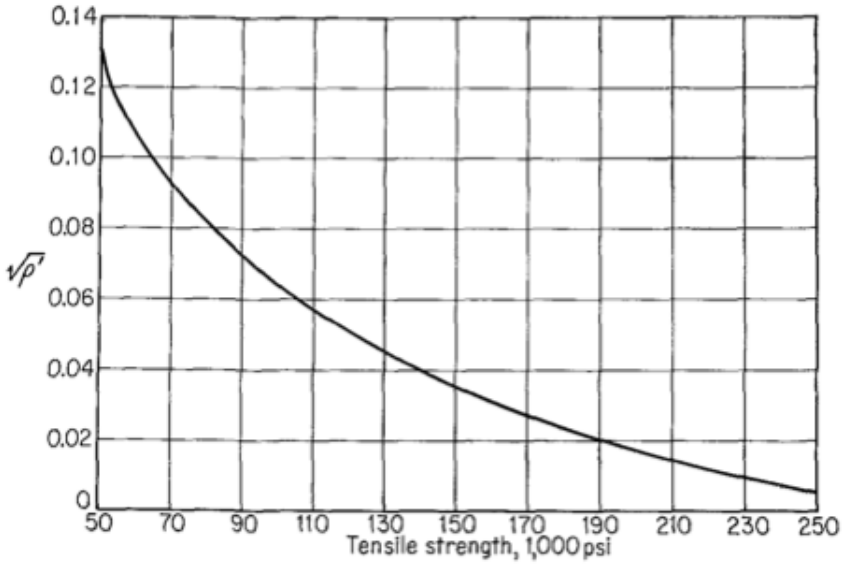

Figure 8: $\sqrt{\rho'}$ as a function of tensile strength of steels. The figure was taken from [11].

$\sigma_{ut}/1000$	α
50	0.015
75	0.010
100	0.007
125	0.005
150	0.0035
200	0.0020
250	0.0013

Figure 9: The relation between the material constant α and the tensile strength of steels. The figure was taken from [12].

how Peterson's formula approaches 1 more rapidly than Neuber's. This implies that by using Peterson's formula, the estimated K_{tf} will approach K_{tn} as the hole diameter increases. It should be pointed out that these ways of estimating q (equations (32) and (33)) are only approximate. As stated in [15], probably none of the available methods of estimating q gives sufficient weight on the effect of size. There are many studies that show that the significance of stress concentrations increases with size, both for static and repeated loading. Therefore, in order to avoid underestimating the value of q, the notch radius, r, was chosen as the outer diameter of the threaded holes. For example, the q for the M8 screw thread was calculated using an r of 8 mm (0.315 inches) in equation (32) and (33).

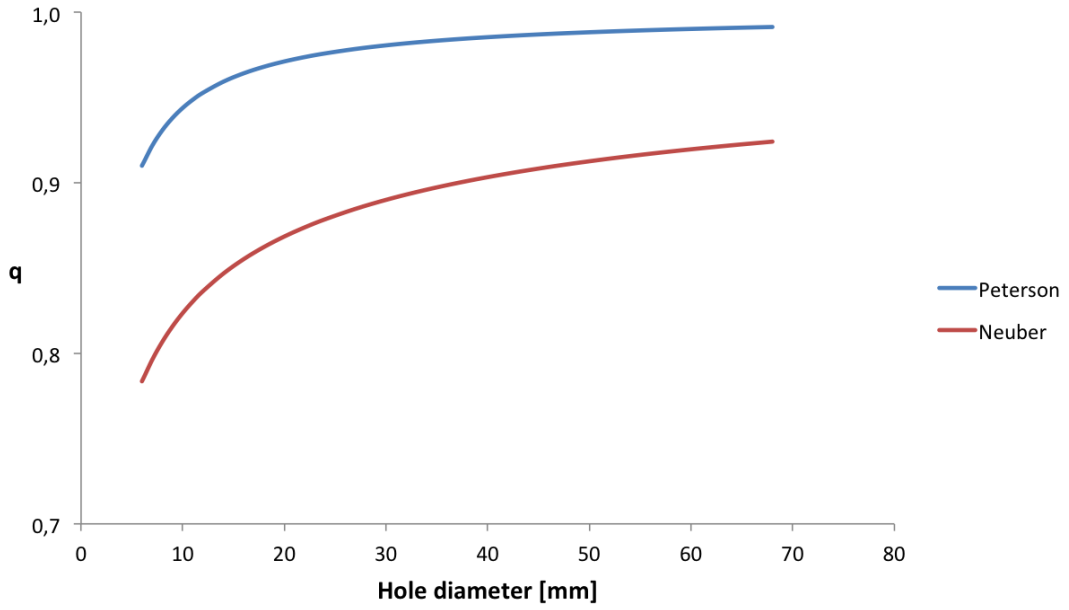

Figure 10: The notch sensitivity index calculated for a structural steel with a tensile strength of $66.7 \cdot 10^3$ psi, using both Neuber's and Peterson's formulas, for the ISO metric screw hole dimensions investigated in this project.

7 Results

For every size of the threaded holes, two static structural analyzes were made in ANSYS; one with the load applied along the x-axis and one along the y-axis. This was to ensure that the lack of perfect symmetry did not affect the location and magnitude of the maximum stress. In addition, a corresponding analysis was made for a plain hole with a diameter equal to the threaded hole's outer diameter. All the ISO metric screw thread dimensions in [6], starting with M6, were analyzed with a coarse pitch, while only a subset of the hole dimensions were investigated for the case of a fine pitch. A summary of all the results can be found in Appendix A.

The results showed that the stress concentration factors, K_{tn}, for the threaded holes were significantly higher than the K_{tn} for the corresponding plain holes. Also, the K_{tn} for the threaded holes with a coarse pitch were higher than for the threaded holes with a fine pitch. No difference in peak stress was found between the two load cases, that is, the maximum stress in the body was the same, regardless if the load was applied in the x or y-direction. The location of the peak stress was consistently found to be on the surface of a thread perpendicular to the direction

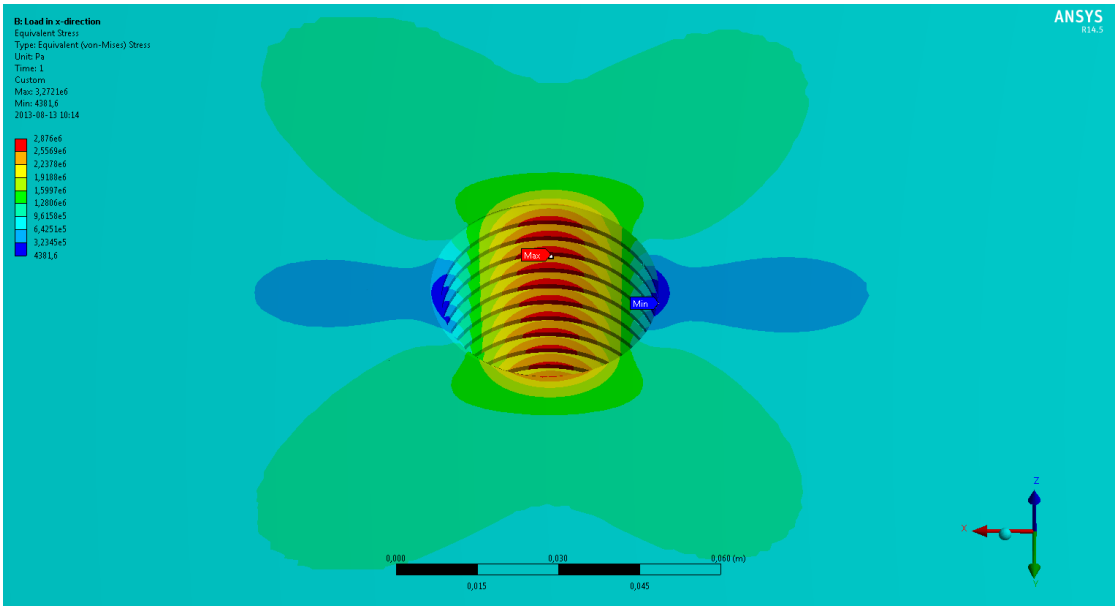

Figure 11: The equivalent stress distribution for an M45 with coarse pitch after a static structural analysis in ANSYS.

of the load, and slightly below the surface of the element. A typical result can be seen in Figure 11, where the locations of the peak stress and the minimum stress are highlighted. One can see that the peak stress appears at a distance down in the hole.

In Figure 12, the resulting stress concentration factors for the threaded holes can be seen together with the corresponding plain holes. The K_{tn} for the coarse threads were about 20 % higher than the plain holes for the smallest dimensions, while, for the biggest dimensions, the difference decreased to about 11 %. For the threaded holes with a fine pitch, the increase in K_{tn} compared to the plain holes was slightly lower; about 16 % for the smaller ones and about 10 % for the biggest dimensions. For both coarse and fine pitch, the tendency is that as the diameter of the hole increases, K_{tn} decreases. Note that this is possible since all dimensions of the solid increase with the same magnitude. In other words, the size of the hole does not increase relative to the size of the solid. For the plain holes, the results follow what could be expected, that is, since all dimensions increase with the same magnitude, K_{tn} remains constant. The reason for the fluctuating pattern for the coarse pitch in Figure 12 is the way the ISO metric thread dimensions change for each hole diameter. Often, the pitch is the same for two or three subsequent hole diameters before the pitch is increased. Therefore, each time the pitch is increased, the result is a small increase in K_{tn} compared to the previous diameter. For the case when

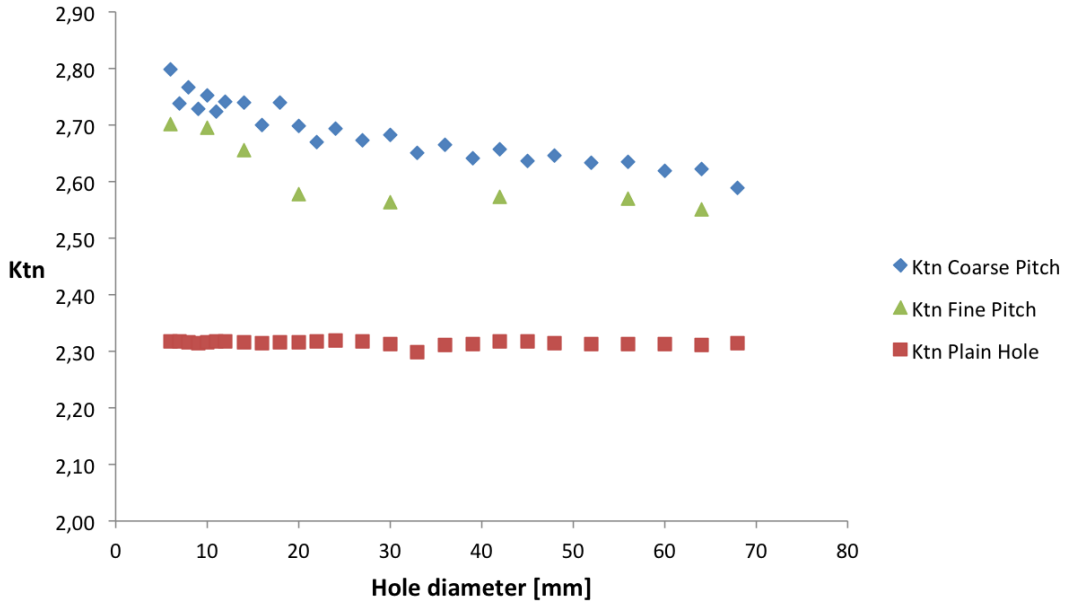

Figure 12: Stress concentration factors, K_{tn}, for threaded holes with coarse and fine pitch, as well as K_{tn} for the corresponding plain holes.

the pitch is held constant for two subsequent diameters, the hole with the bigger diameter will have a slightly lower K_{tn}.

For the fatigue analysis, the fatigue notch factor, K_{tf}, was calculated according to equation (31). Both Neuber's (32) and Peterson's formulas (33) were used to determine the notch sensitivity index q. In Figure 13, K_{tf} is plotted based on Neuber's and Peterson's formulations of q respectively. One can see that Peterson's formula overall gives a higher estimate of K_{tf} than Neuber's formula. Which estimate is the more accurate one is impossible to tell without access to experimental data. However, Peterson's formula is obviously more conservative in design purposes. Since there was an uncertainty in the actual magnitude of K_{tf}, a comparison between the predicted reduction in fatigue strength between the two ways of calculating K_{tf} was made. By using the definition of the fatigue notch factor in equation (29), the following expression was derived

$$\sigma_n^{thread} = \frac{K_{tf}^{plain}}{K_{tf}^{thread}} \cdot \sigma_n^{plain} \tag{34}$$

where σ_n^{thread} and σ_n^{plain} are the fatigue strengths of a threaded hole and a plain hole respectively, and K_{tf}^{thread} and K_{tf}^{plain} are the corresponding fatigue notch factors.

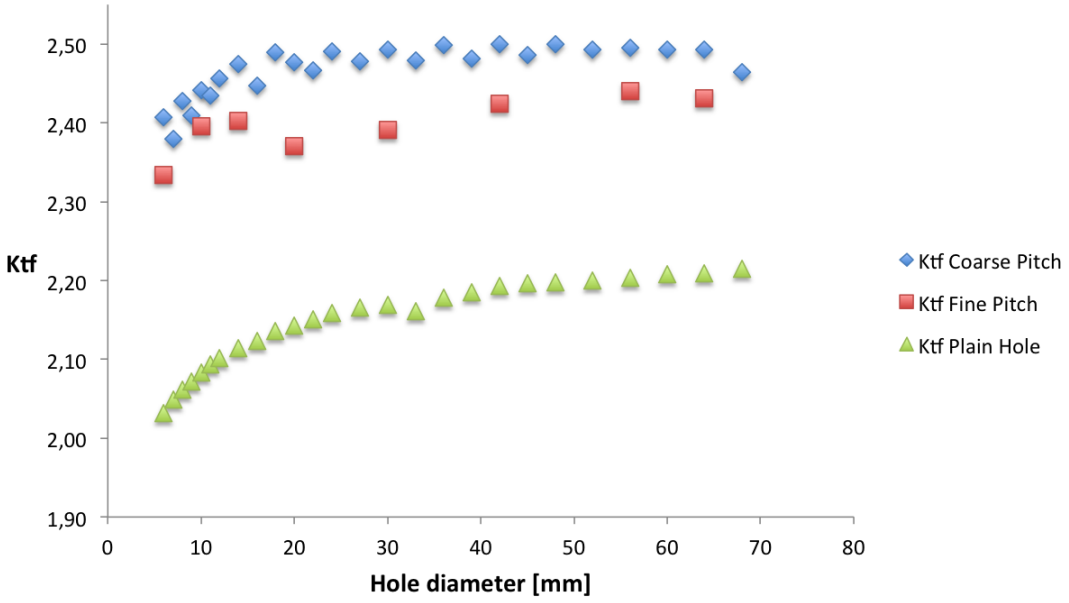

(a) Neuber

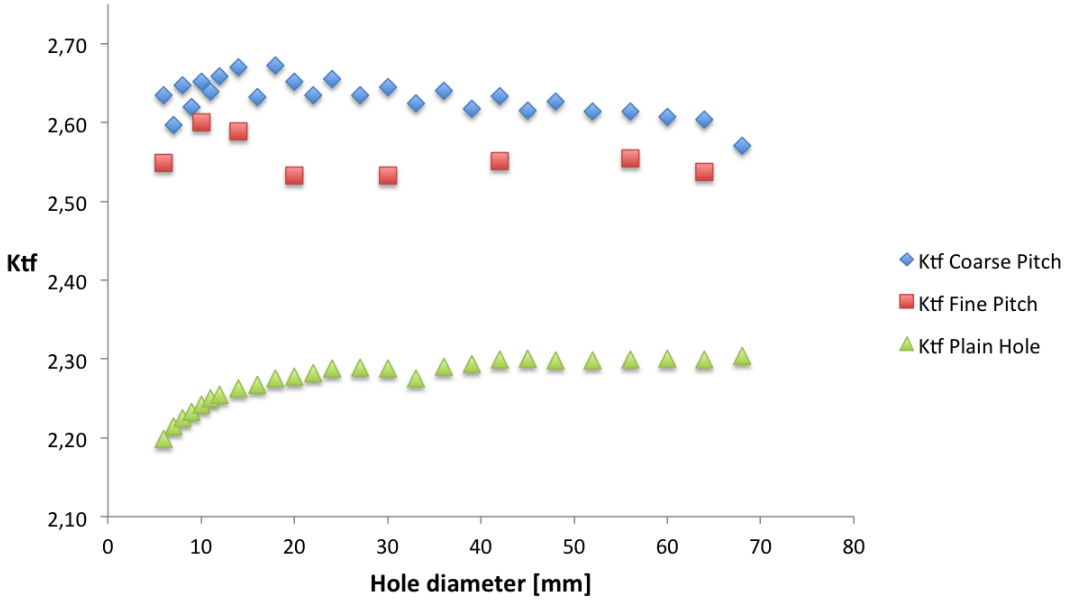

(b) Peterson

Figure 13: Fatigue notch factors, K_{tf}, for threaded and plain holes, calculated with Neuber's and Peterson's formulas respectively.

The subscript n is to denote that both fatigue strengths are for notched specimen. The percentage decrease in fatigue strength of a threaded hole compared to a plain hole could then be expressed as

$$\Delta_{\%} = 1 - \frac{K_{tf}^{plain}}{K_{tf}^{thread}} \tag{35}$$

By using equation (35), the expected reduction in fatigue strength according to Neuber's formula could be compared with the expected reduction according to Peterson. Figure 14 shows that, when put in terms of percentage change in fatigue strength, the two estimations give roughly the same results. Both predict that the fatigue strength of an M6 is around 16 % lower than a plain hole of equal size for a structural steel with a tensile strength of 460 MPa ($66.7 \cdot 10^3$ psi). The reduction in fatigue strength drops as the size of the hole increases and for an M68, the reduction is only about 10 %. Note that the difference between the two measures becomes smaller for the large holes. For the threaded holes with a fine pitch, the percentage reduction in fatigue strength varied from about 14 % for the M6 to about 9 % for the M64.

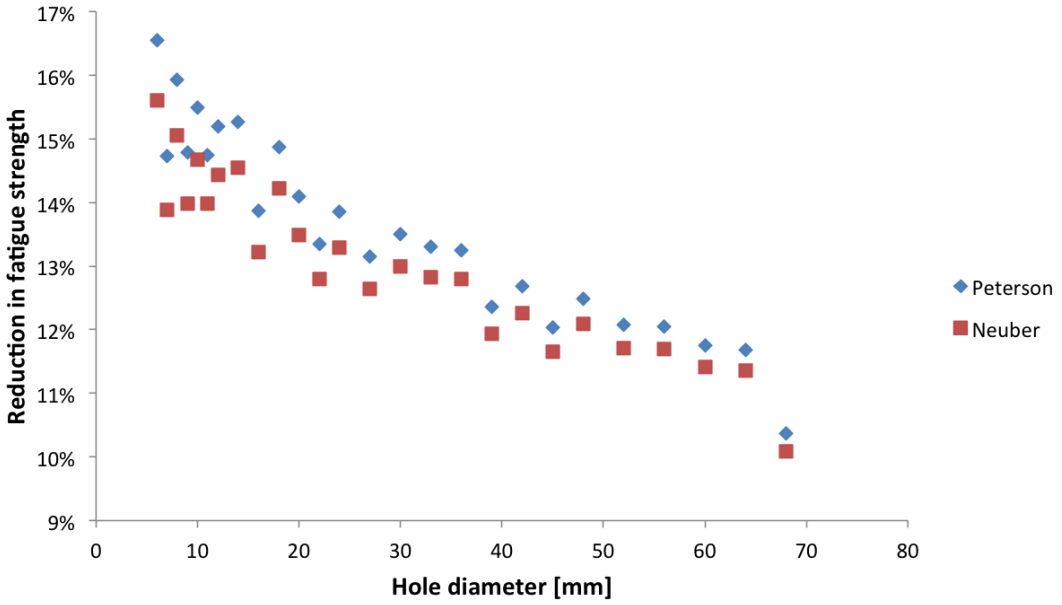

Figure 14: The percentage decrease in fatigue strength for a threaded hole compared to a plain hole, calculated with both Neuber's and Peterson's estimations of q. Only the ISO metric threads with a coarse pitch are plotted.

8 Conclusions

In this project, the stress concentration factors, K_{tn}, as well as the fatigue notch factors, K_{tf}, for threaded holes located in a rectangular body of structural steel with a tensile strength of 460 MPa, have been investigated. For the threaded holes, K_{tn} was found to be significantly higher than the corresponding K_{tn} for plain holes. For ISO metric screw threads with a coarse pitch, the increase in K_{tn}, compared to the plain holes, varied from 20 % for an M6 to an 11 % increase for an M68. For the threaded holes with a fine pitch, the increase in K_{tn} varied from 16 % for an M6 to a 10 % increase for an M64. As the size of the hole and the surrounding body increased, the stress concentration factor decreased. When two threaded holes had different diameters but the same pitch, the hole with the bigger diameter had a lower K_{tn}.

The resulting magnitude of the fatigue notch factor, K_{tf}, depends on what estimate of the notch sensitivity index, q, that is being applied. Peterson's formula is more conservative, that is, it predicts a higher value of q than Neuber, and could therefore be suitable in design purposes. However, the percentage reduction in fatigue strength of threaded holes, compared to plain holes, does not depend greatly on what measure is being used for q. Both Neuber's and Peterson's formulas gave similar results. The calculated reduction in fatigue strength for threaded holes with a coarse pitch varied from about 16 % for the smallest diameter investigated (M6) to about 10 % for the biggest (M68). The corresponding reduction for threaded holes with a fine pitch varied from about 14 % for the smallest diameter (M6) to about 9 % for the biggest (M64). As the size of the hole and the surrounding body increased, the percentage reduction in fatigue strength for threaded holes, compared to plain holes, decreased.

9 Recommendations for Further Research

To obtain a deeper understanding of the thread's effect on the stress concentration factor, as well as the fatigue properties, different load cases must be investigated. Bending and shear stress was excluded in this project and to examine the stress distribution for these load cases would be a natural extension to the current research. Furthermore, the relative dimensions of the solid and the threaded holes were kept constant in the simulations. It would be interesting to see what happens if the block size is kept constant, while the hole diameter is increased. At some point, the size of the hole, relative to the block, will be big enough to, in theory, affect an area bigger than the surrounding body. This could definitely be the case

in machine parts where the threaded holes are located close to an edge.

A modification at the top of the threaded holes was considered during the project, where the holes would get a chamfer. This would move the sharp edge, created by the threads, further down. Since the maximum stress occurs at a distance down in the hole, a chamfer could increase the stress concentration factor if the location of the sharp edge coincide with the location of the maximum stress. Moreover, to investigate the stress concentration factors of chamfered threaded holes would be meaningful since they frequently occur in the industry.

A Table of all results

Model	d (mm)	r (in.)	q_{Neuber}	$q_{Peterson}$	Coarse Pitch									
					Load in x					Load in y				
					σ_{max} (Pa)	K_{tg}	K_{tn}	K_f^{Neuber}	$K_f^{Peterson}$	σ_{max} (Pa)	K_{tg}	K_{tn}	K_f^{Neuber}	$K_f^{Peterson}$
M6	6	0,118	0,783	0,910	3,05E+06	3,05	2,80	2,41	2,63	3,05E+06	3,05	2,80	2,41	2,64
M7	7	0,138	0,796	0,922	2,98E+06	2,98	2,73	2,38	2,60	2,99E+06	2,99	2,74	2,38	2,60
M8	8	0,157	0,807	0,931	3,02E+06	3,02	2,77	2,43	2,65	3,02E+06	3,02	2,77	2,43	2,64
M9	9	0,177	0,816	0,938	2,98E+06	2,98	2,73	2,41	2,62	2,98E+06	2,98	2,73	2,41	2,62
M10	10	0,197	0,824	0,944	3,00E+06	3,00	2,75	2,44	2,65	3,00E+06	3,00	2,75	2,44	2,65
M11	11	0,217	0,830	0,949	2,98E+06	2,98	2,73	2,43	2,64	2,97E+06	2,97	2,72	2,43	2,64
M12	12	0,236	0,836	0,953	2,99E+06	2,99	2,74	2,46	2,66	2,99E+06	2,99	2,74	2,46	2,66
M14	14	0,276	0,847	0,959	2,99E+06	2,99	2,74	2,47	2,67	2,99E+06	2,99	2,74	2,47	2,67
M16	16	0,315	0,855	0,964	2,94E+06	2,94	2,69	2,45	2,63	2,95E+06	2,95	2,70	2,45	2,64
M18	18	0,354	0,862	0,968	2,98E+06	2,98	2,73	2,49	2,67	2,99E+06	2,99	2,74	2,50	2,68
M20	20	0,394	0,869	0,971	2,95E+06	2,95	2,70	2,48	2,65	2,94E+06	2,94	2,70	2,47	2,65
M22	22	0,433	0,874	0,974	2,92E+06	2,92	2,68	2,47	2,63	2,91E+06	2,91	2,67	2,46	2,63
M24	24	0,472	0,879	0,976	2,94E+06	2,94	2,70	2,49	2,66	2,94E+06	2,94	2,69	2,49	2,65
M27	27	0,531	0,885	0,978	2,91E+06	2,91	2,67	2,48	2,63	2,92E+06	2,92	2,67	2,48	2,64
M30	30	0,591	0,890	0,981	2,92E+06	2,92	2,68	2,49	2,65	2,93E+06	2,93	2,68	2,50	2,65
M33	33	0,650	0,895	0,982	2,90E+06	2,90	2,65	2,48	2,62	2,89E+06	2,89	2,65	2,48	2,62
M36	36	0,709	0,899	0,984	2,91E+06	2,91	2,67	2,50	2,64	2,91E+06	2,91	2,67	2,50	2,64
M39	39	0,768	0,902	0,985	2,88E+06	2,88	2,64	2,48	2,62	2,88E+06	2,88	2,64	2,48	2,62
M42	42	0,827	0,905	0,986	2,90E+06	2,90	2,66	2,50	2,63	2,90E+06	2,90	2,66	2,50	2,63
M45	45	0,886	0,908	0,987	2,88E+06	2,88	2,64	2,49	2,62	2,88E+06	2,88	2,64	2,49	2,61
M48	48	0,945	0,911	0,988	2,89E+06	2,89	2,65	2,50	2,63	2,89E+06	2,89	2,65	2,50	2,63
M52	52	1,024	0,914	0,989	2,87E+06	2,87	2,63	2,49	2,61	2,87E+06	2,87	2,63	2,49	2,61
M56	56	1,102	0,917	0,989	2,87E+06	2,87	2,63	2,50	2,61	2,87E+06	2,87	2,63	2,50	2,62
M60	60	1,181	0,920	0,990	2,86E+06	2,86	2,62	2,49	2,61	2,86E+06	2,86	2,62	2,49	2,60
M64	64	1,260	0,922	0,991	2,86E+06	2,86	2,62	2,49	2,60	2,86E+06	2,86	2,62	2,50	2,61
M68	68	1,339	0,924	0,991	2,82E+06	2,82	2,58	2,46	2,57	2,82E+06	2,82	2,59	2,47	2,58

	Fine Pitch										Plain hole				
	Load in x					Load in y									
Model	σ_{max} (Pa)	K_{tg}	K_{tn}	K_f^{Neuber}	$K_f^{Peterson}$	σ_{max} (Pa)	K_{tg}	K_{tn}	K_f^{Neuber}	$K_f^{Peterson}$	σ_{max} (Pa)	K_{tg}	K_{tn}	K_f^{Neuber}	$K_f^{Peterson}$
M6	2,95E+06	2,95	2,70	2,33	2,55	2,94E+06	2,94	2,70	2,33	2,54	2,57E+06	2,57	2,32	2,03	2,20
M7											2,57E+06	2,57	2,32	2,05	2,21
M8											2,57E+06	2,57	2,32	2,06	2,23
M9											2,57E+06	2,57	2,31	2,07	2,23
M10	2,94E+06	2,94	2,69	2,40	2,60	2,95E+06	2,95	2,70	2,40	2,61	2,57E+06	2,57	2,32	2,08	2,24
M11											2,57E+06	2,57	2,32	2,09	2,25
M12											2,57E+06	2,57	2,32	2,10	2,25
M14	2,90E+06	2,90	2,66	2,40	2,59	2,90E+06	2,90	2,65	2,40	2,59	2,57E+06	2,57	2,32	2,11	2,26
M16											2,57E+06	2,57	2,31	2,12	2,27
M18											2,57E+06	2,57	2,32	2,14	2,27
M20	2,81E+06	2,81	2,58	2,37	2,53	2,82E+06	2,82	2,58	2,37	2,54	2,57E+06	2,57	2,32	2,14	2,28
M22											2,57E+06	2,57	2,32	2,15	2,28
M24											2,58E+06	2,58	2,32	2,16	2,29
M27											2,57E+06	2,57	2,32	2,17	2,29
M30	2,80E+06	2,80	2,56	2,39	2,53	2,80E+06	2,80	2,56	2,39	2,53	2,57E+06	2,57	2,31	2,17	2,29
M33											2,55E+06	2,55	2,30	2,16	2,28
M36											2,57E+06	2,57	2,31	2,18	2,29
M39											2,57E+06	2,57	2,31	2,19	2,29
M42	2,81E+06	2,81	2,57	2,42	2,55	2,81E+06	2,81	2,57	2,42	2,55	2,57E+06	2,57	2,32	2,19	2,30
M45											2,57E+06	2,57	2,32	2,20	2,30
M48											2,57E+06	2,57	2,31	2,20	2,30
M52											2,57E+06	2,57	2,31	2,20	2,30
M56	2,80E+06	2,80	2,57	2,44	2,55	2,81E+06	2,81	2,57	2,44	2,56	2,57E+06	2,57	2,31	2,20	2,30
M60											2,57E+06	2,57	2,31	2,21	2,30
M64	2,78E+06	2,78	2,55	2,43	2,54	2,78E+06	2,78	2,55	2,43	2,54	2,57E+06	2,57	2,31	2,21	2,30
M68											2,57E+06	2,57	2,32	2,22	2,30

B Tables of data for coarse and fine screw threads

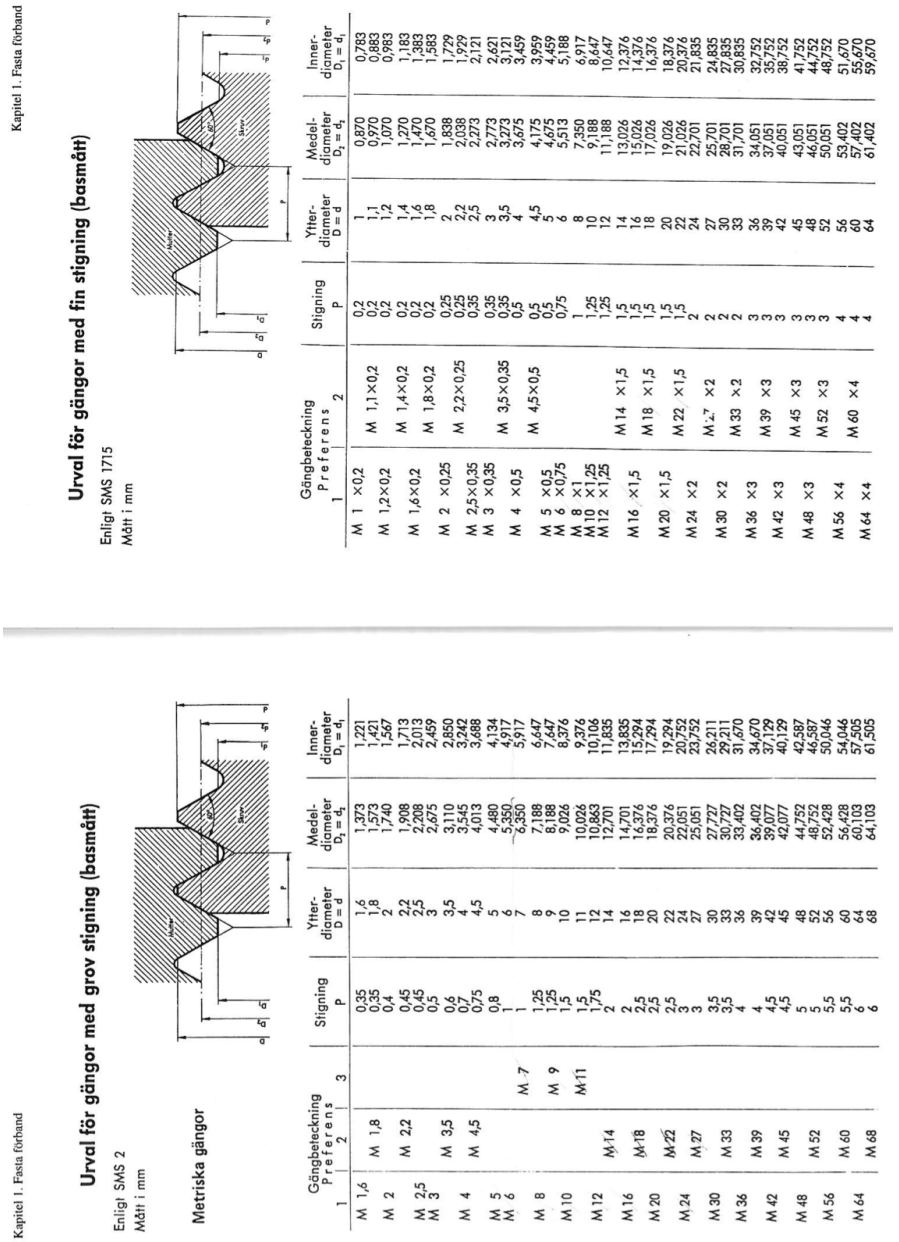

Kapitel 1. Fästa förband

Urval för gängor med fin stigning (basmått)

Enligt SMS 1715

Mått i mm

Gängbeteckning Preferens 1	Gängbeteckning Preferens 2	Stigning P	Ytter-diameter D = d	Medel-diameter $D_2 = d_2$	Inner-diameter $D_1 = d_1$
M 1 ×0,2		0,2	1	0,870	0,783
	M 1,1×0,2	0,2	1,1	0,970	0,883
M 1,2×0,2		0,2	1,2	1,070	0,983
	M 1,4×0,2	0,2	1,4	1,270	1,183
M 1,6×0,2		0,2	1,6	1,470	1,383
	M 1,8×0,2	0,2	1,8	1,670	1,583
M 2 ×0,25		0,25	2	1,838	1,729
	M 2,2×0,25	0,25	2,2	2,038	1,929
M 2,5×0,35		0,35	2,5	2,273	2,121
M 3 ×0,35		0,35	3	2,773	2,621
	M 3,5×0,35	0,35	3,5	3,273	3,121
M 4 ×0,5		0,5	4	3,675	3,459
	M 4,5×0,5	0,5	4,5	4,175	3,959
M 5 ×0,5		0,5	5	4,675	4,459
M 6 ×0,75		0,75	6	5,513	5,188
M 8 ×1		1	8	7,350	6,917
M 10 ×1,25		1,25	10	9,188	8,647
M 12 ×1,25		1,25	12	11,188	10,647
	M 14 ×1,5	1,5	14	13,026	12,376
M 16 ×1,5		1,5	16	15,026	14,376
	M 18 ×1,5	1,5	18	17,026	16,376
M 20 ×1,5		1,5	20	19,026	18,376
	M 22 ×1,5	1,5	22	21,026	20,376
M 24 ×2		2	24	22,701	21,835
	M 27 ×2	2	27	25,701	24,835
M 30 ×2		2	30	28,701	27,835
	M 33 ×2	2	33	31,701	30,835
M 36 ×3		3	36	34,051	32,752
	M 39 ×3	3	39	37,051	35,752
M 42 ×3		3	42	40,051	38,752
	M 45 ×3	3	45	43,051	41,752
M 48 ×3		3	48	46,051	44,752
	M 52 ×3	3	52	50,051	48,752
M 56 ×4		4	56	53,402	51,670
	M 60 ×4	4	60	57,402	55,670
M 64 ×4		4	64	61,402	59,670

Kapitel 1. Fästa förband

Urval för gängor med grov stigning (basmått)

Enligt SMS 2

Mått i mm

Metriska gängor

Gängbeteckning Preferens 1	Gängbeteckning Preferens 2	Gängbeteckning Preferens 3	Stigning P	Ytter-diameter D = d	Medel-diameter $D_2 = d_2$	Inner-diameter $D_1 = d_1$
M 1,6			0,35	1,6	1,373	1,221
	M 1,8		0,35	1,8	1,573	1,421
M 2			0,4	2	1,740	1,567
	M 2,2		0,45	2,2	1,908	1,713
M 2,5			0,45	2,5	2,208	2,013
M 3			0,5	3	2,675	2,459
	M 3,5		0,6	3,5	3,110	2,850
M 4			0,7	4	3,545	3,242
	M 4,5		0,75	4,5	4,013	3,688
M 5			0,8	5	4,480	4,134
M 6			1	6	5,350	4,917
		M 7	1	7	6,350	5,917
M 8			1,25	8	7,188	6,647
		M 9	1,25	9	8,188	7,647
M 10			1,5	10	9,026	8,376
		M 11	1,5	11	10,026	9,376
M 12			1,75	12	10,863	10,106
	M 14		2	14	12,701	11,835
M 16			2	16	14,701	13,835
	M 18		2,5	18	16,376	15,294
M 20			2,5	20	18,376	17,294
	M 22		2,5	22	20,376	19,294
M 24			3	24	22,051	20,752
	M 27		3	27	25,051	23,752
M 30			3,5	30	27,727	26,211
	M 33		3,5	33	30,727	29,211
M 36			4	36	33,402	31,670
	M 39		4	39	36,402	34,670
M 42			4,5	42	39,077	37,129
	M 45		4,5	45	42,077	40,129
M 48			5	48	44,752	42,587
	M 52		5	52	48,752	46,587
M 56			5,5	56	52,428	50,046
	M 60		5,5	60	56,428	54,046
M 64			6	64	60,103	57,505
	M 68		6	68	64,103	61,505

ISO-standard for metric screw threads taken from, [6].

C How to use the script file

Below is a description on how to use the script for dividing the body into different parts.

1. Import your CAD-model to Designmodeler
2. Make sure that the coordinate system is according to the one used in Figure 15.

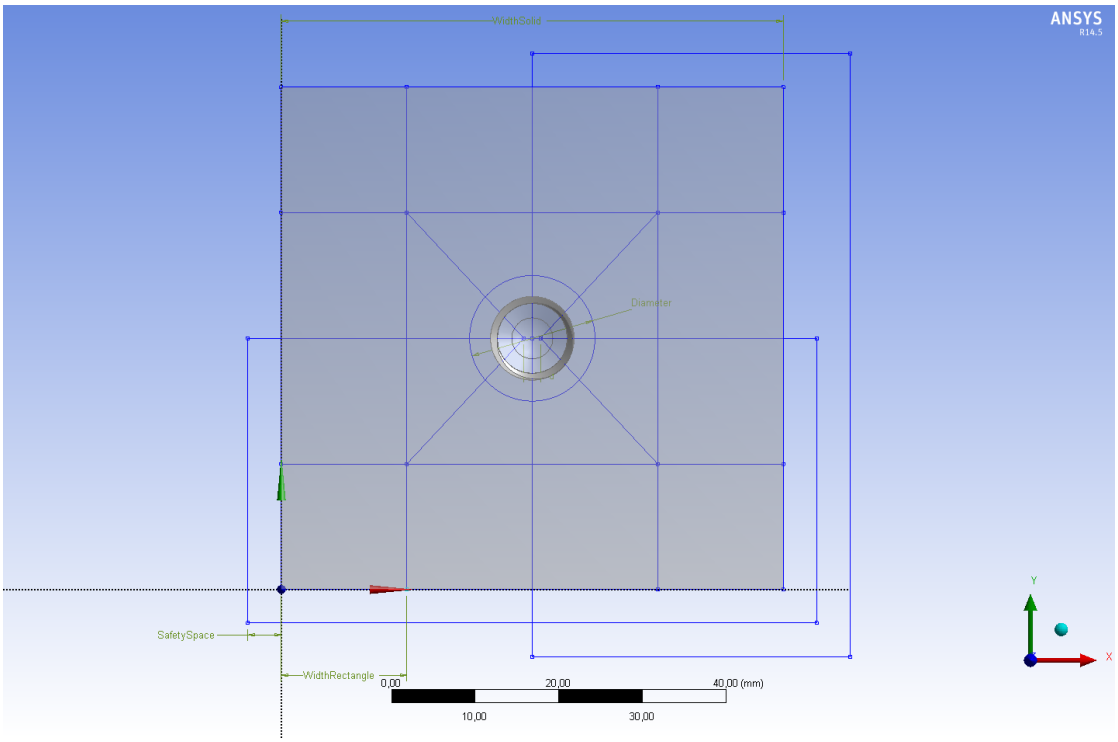

Figure 15

   - If not, create a new coordinate system according to the one in Figure 15. This is done by creating a new plane in Designmodeler.
3. Choose the coordinate system that you want to generate the sketch in (planes in Designmodeler), then
   - Press File → Run Script → "Generate sketch threaded hole Improved".
   - The file is in $C:\backslash ProgramFiles\backslash ANSYSInc\backslash v145\backslash aisol\backslash DesignSpace\backslash DSPages\backslash macros$, which is the default path.

4. The sketch should be visible now. Change the dimensions of the sketch to fit your model. Note that the order in which you change the dimensions might affect whether you get an error or not. OBS! You might have to increase the parameter d in order to avoid contact surfaces. The general way of changing the dimensions that works most of the times is: WidthSolid$\rightarrow$ WidthRectangle $\rightarrow$ Diameter.
    - Diameter: The diameter of the cylinder surrounding the threaded hole, which later will contain the mesh with the smallest elements.
    - WidthRectangle: The width of the rectangles closest to the boundaries of the body, which later will contain the mesh with the largest elements.
    - WidthSolid: The body's outer dimensions, the size of the block containing the threaded hole.
    - Safety space: No need to change
    - d: Make sure that d is bigger than the diameter of the circle at the bottom of the hole.
5. Make an *Extrude* for each sketch in order to divide the body into different parts. Choose
    - Geometry: Actual sketch (Sketch 4, 5, or 6)
    - Operation: Slice material
    - Extent type: Through all
6. You should now have 28 "bodies". It is important to merge all the bodies into one part, which is done by highlighting all the bodies and choose *Form new part.*

References

[1] Klaus-Jürgen Bathe. *Finite element procedures*. Prentice hall Englewood Cliffs, 1996.

[2] Bruce Boardman. Fatigue resistance of steels. *ASM International, Metals Handbook. Tenth Edition*, 1:673–688, 1990.

[3] Allan F Bower. *Applied mechanics of solids*. CRC press, 2011.

[4] Longchao Dai and Junjie Gong. The three-dimensional stress field in an arbitrary thickness plate holding a circular hole. *International Journal of Mechanic Systems Engineering*.

[5] Prakash Mahaedo Dixit and Uday S Dixit. *Modeling of metal forming and machining processes: by finite element and soft computing methods*. Springer, 2008.

[6] Lars Eriksson, Anders Folkeson, and Lars Hagman mfl. *Maskinelement Handbok*. Nordstedts, 1994.

[7] Paul Kuhn and Herbert F Hardrath. An engineering method for estimating notch-size effect in fatigue tests on steel. *NACA Tech*, 1952.

[8] Zhenhuan Li, Wanlin Guo, and Zhenbang Kuang. Three-dimensional elastic stress fields near notches in finite thickness plates. *International Journal of Solids and Structures*, 37, 2000.

[9] Per-Olof Persson. Mesh size functions for implicit geometries and pde-based gradient limiting. *Engineering with Computers*, 22(2):95–109, 2006.

[10] Rudolph Earl Peterson. *Stress Concentration Factors*. John Wiley & Sons, 1974.

[11] Rudolph Eearl Peterson. *Notch sensitivity*. McGraw-Hill New York, 1959.

[12] Walter D Pilkey and Deborah F Pilkey. *Peterson's stress concentration factors*. John Wiley & Sons, 2008.

[13] E. Sternberg and M. A. Sadowski. Three-dimensional solution for the stress concentration around a circular hole in a plate of arbitrary thickness. *Transactions of ASME Applied Mechanics Section*, 71, 1949.

[14] Chia-hsiang Yen and Thomas James Dolan. *A Critical Review of the Criteria for Notch-sensitivity in Fatigue of Metals*. University of Illinois, 1952.

[15] Warren C Young. *Roark's formulas for stress and strain, 6th edition.* McGraw-Hill, 1989.

[16] Olgierd Cecil Zienkiewicz and Robert Leroy Taylor. *The finite element method Volume 1: The Basis.* Butterworth-Heinemann, 2000.